J Nanostruct 16(3): 3094-3111, Summer 2026

RESEARCH PAPER

# Synthesis, Characterization, Biological Activity, Cytotoxicity (MTT Assay), and Antioxidant Evaluation of a Novel Ligand (BHDPE) and Its Ni(II) Complex

*Yareeb Jwad Sahar* [1]*, *Abbas Fadhil Yasir* [2]

[1] *Department of Chemistry, College of Science, University of Al-Qadisiyah, Al-Qadisiyah, Iraq*

[2] *Department of Chemistry, General Directorate of Education Al-Muthanna, Al-Muthanna, Iraq*

**ARTICLE INFO**

***Article History:***
*Received 09 March 2026*
*Accepted 11 May 2026*
*Published 01 July 2026*

***Keywords:***
*Antioxidant*
*Biological activity*
*MCF-7*
*Molecular Docking*
*Schiff base*

**ABSTRACT**

A novel ligand, (E)-2-(2-(benzo[d]oxazol-2-yl)hydrazono)-1,2-diphenylethan-1-ol (BHDPE), was synthesized via a two-step procedure. In the first step, the intermediate compound (A), 2-hydrazinylbenzo[d] oxazole, was prepared by reacting 2-mercaptobenzoxazole with hydrazine hydrate in an ethanolic medium. In the second step, the BHDPE ligand was obtained by condensation of intermediate (A) with benzoin. The Ni(II) complex was synthesized in a 1:2 metal-to-ligand molar ratio. The Ni(II) complex was determined to possess an octahedral geometry. The structural elucidation of the ligand and its complex was accomplished using FT-IR, $^{1}$H-$^{3}$C NMR, and UV-Vis spectroscopy, in conjunction with molar conductivity measurements, elemental analysis (CHN), atomic absorption spectroscopy, and magnetic susceptibility studies. The synthesized compounds exhibited significant antibacterial activity against selected bacterial strains and notable antioxidant capacity against free radicals. The BHDPE ligand and Nickel (II) complex exhibited high toxicity against MCF-7 with high different values between $IC_{50}$ against infection cells and healthy cells Furthermore, molecular docking studies revealed favorable binding affinity of the synthesized compounds toward the target protein (3FC2). The ligand exhibited a particularly strong binding affinity, indicative of a stable interaction with the active site of the target protein.

**How to cite this article**
*Sahar Y., Yasir A. Synthesis, Characterization, Biological Activity, Cytotoxicity (MTT Assay), and Antioxidant Evaluation of a Novel Ligand (BHDPE) and Its Ni(II) Complex. J Nanostruct, 2026; 16(3):3094-3111. DOI: 10.22052/JNS.2026.03.007*

## INTRODUCTION

Benzoxazoles are heterocyclic aromatic organic compounds consisting of a benzene ring fused to an oxazole ring. They have the molecular formula $C_7H_5NO$ and typically exist as white to pale yellow crystalline solids. These compounds exhibit a relatively low melting point (30–33 °C) and are sparingly soluble in water, yet readily soluble in common organic solvents such as ethanol [1]. Benzoxazole can be synthesized via a straightforward reaction of o-aminophenol with carboxylic acid in the presence of polyphosphoric acid (PPA) as a catalyst [2]. Numerous benzoxazole derivatives have been employed in pharmaceutical applications owing to their diverse pharmacological properties, including antibacterial, antidepressant, antispasmodic, antimicrobial, antifungal, and cardiovascular activities, as well as their

* *Corresponding Author Email: Yarub.Jwad@qu.edu.iq*

utility as anesthetic agents[3] Benzoxazole has been frequently incorporated into Schiff base frameworks, which feature the characteristic azomethine (C=N) functional group[4], Schiff bases were first reported by the German chemist Hugo Schiff through the condensation reaction of primary amines with' aldehydes or ketones [5]. Recent studies have demonstrated that sulfur-promoted oxidative rearrangement coupling between o-aminophenols and ketones provides an efficient route for the synthesis of 2-alkylbenzoxazoles under mild conditions [6].

## MATERIALS AND METHODS

All chemicals and reagents were procured from Aldrich, Merck, HIMEDIA, and BDH, and were used without further purification. UV-Vis spectra in the 200–1000 nm range were recorded using a Shimadzu UV-165PCS spectrophotometer. $^{1}H$, $C^{13}$ -NMR spectra were acquired at 300 MHz on the Fourier Transform Varian Spectrometer in DMSO-d6. FT-IR spectra were recorded in the 400–4000 $cm^{-1}$ range using a Shimadzu FT-IR 8400S spectrophotometer. Melting points were determined using a Stuart melting point apparatus. Magnetic susceptibility measurements were performed at room temperature using a Magnetic Susceptibility Balance (MSB-MKI). Metal content in the complexes was determined by flame atomic absorption spectroscopy (Shimadzu AA-6300), and elemental analysis (C, H, N) was performed using a Shimadzu EA-300 elemental analyzer.

### *Preparation of The Ligand*

The ligand (BHDPE) was synthesized in two sequential steps. In the first step, 2-hydrazinylbenzoxazole (compound A) was prepared by dissolving 2-mercaptobenzoxazole

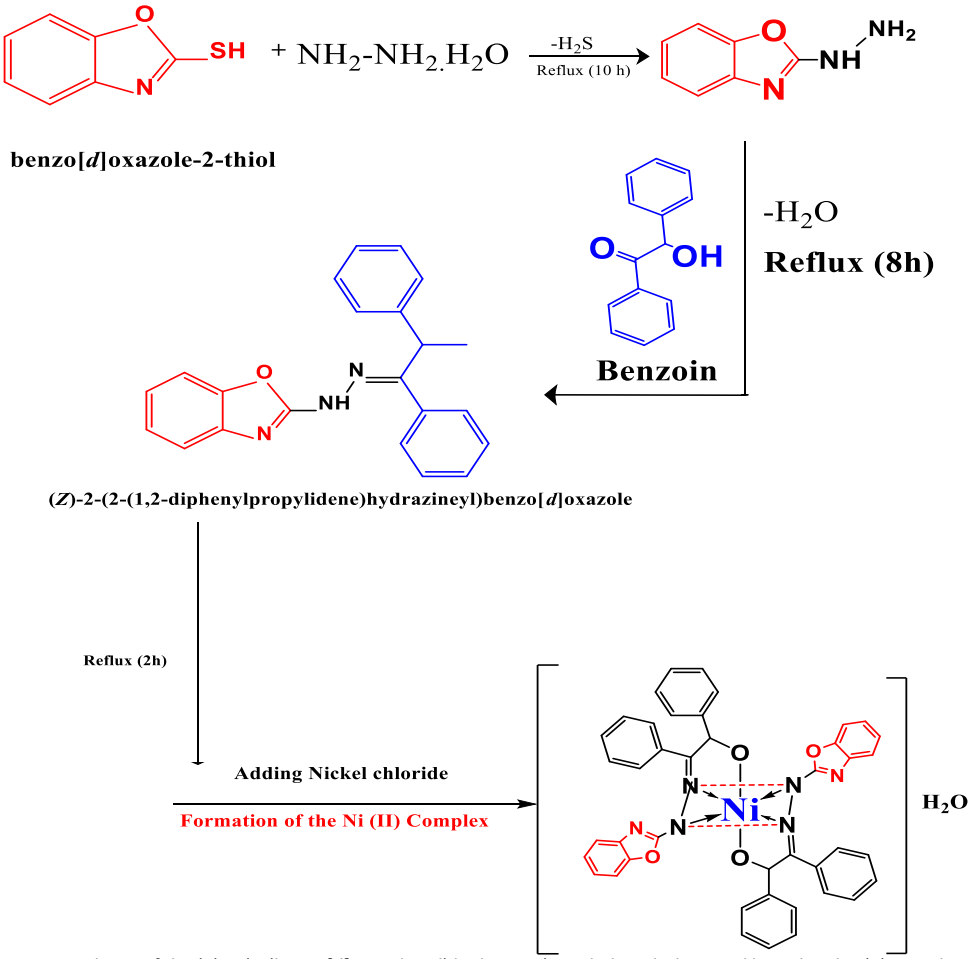


Fig. 1. Synthesis of the (E)-2-(2-(benzo[d]oxazol-2-yl) hydrazone)-1,2diphenylethan-1-ol ligand and Ni(II) complex.

(2.00 g, 13.2 mmol) in absolute ethanol (25 mL), followed by the dropwise addition of hydrazine hydrate (0.66 g, 13.2 mmol) dissolved in absolute ethanol (25 mL). The reaction mixture was heated under reflux for 10 h, then cooled to room temperature, filtered, and the precipitate was collected. The crude product was recrystallized from absolute ethanol, dried under vacuum, and collected, affording compound A in 85% yield (m.p. 169–171 °C). The ligand (E)-2-(2-(benzo[d] oxazol-2-yl) hydrazone)-1,2diphenylethan-1-ol (BHDPE) was made by dissolving (1.3 gm, 8.71 mmole) of the A-compound in 25 ml of ethanol with constant stirring. A solution of benzoin (1.85 g, 8.71 mmol) in ethanol (25 mL) was then added, along with 5–6 drops of concentrated hydrochloric acid as catalyst, and the mixture was refluxed for 8 h before being cooled to room temperature. The resulting precipitate was filtered, dried, and recrystallized from absolute ethanol. As shown in Fig. 1, The product had an 83% yield and a melting point of (BHDPE) ligand was 133 $^{0}$C.

*Synthesis of the Ni (II) Complex for (BHDPE) ligand*

The Ni(II) complex was prepared in a 1:2 (M:L) molar ratio according to the following procedure. A solution of BHDPE ligand (0.13 g, 0.37 mmol) in absolute ethanol (10 mL) was added dropwise to a solution of nickel(II) chloride (0.185 mmol) in absolute ethanol (10 mL), and the resulting mixture was refluxed with continuous stirring for 2 h. The mixture was subsequently cooled, filtered, and the product was dried and recrystallized from absolute ethanol.

*Measuring antioxidant capacity*

The antioxidant activity of the synthesized compounds was evaluated against the stable free radical 2,2-diphenyl-1-picrylhydrazyl (DPPH). This was accomplished by dissolving 1 mL of each compound in DMSO at various concentrations (3.9–500 µg/mL). Subsequently, 1 mL of 0.1 mM DPPH solution in methanol was added to each test solution of the BHDPE ligand and Ni(II) complex. The reaction mixtures were incubated at room temperature in the dark for 30 min. A color change from violet to light yellow was observed, indicating radical scavenging activity. The absorbance was measured at 517 nm using a UV-Vis spectrophotometer. Next, each compound's RSA% (percent radical scavenging activity) is computed. The substances are contrasted with ascorbic acid dissolved in DMSO at equivalent concentrations [7].

*Antibacterial activity*

The antibacterial activity of the synthesized compounds was evaluated against selected bacterial strains. The test organisms included the Gram-positive bacterium Staphylococcus aureus and the Gram-negative bacterium Escherichia coli, which are among the most commonly encountered pathogenic bacterial species. Stock solutions of all synthesized compounds were prepared by dissolving them in dimethyl sulfoxide (DMSO) at a concentration of 1000 ppm, followed by serial dilution with DMSO. Additional concentrations of 250 and 500 ppm were prepared. The agar well diffusion method was employed using Mueller-Hinton agar (MH) (Difco, Detroit, MI). The medium was used for culturing the bacterial strains. Under sterile conditions, 100 µL of each prepared compound solution in DMSO (1%) was dispensed into the wells using calibrated micropipettes. An equivalent volume of DMSO was used as the negative control. Inhibition was measured in millimeters after a 37°C incubation period. The activity then is measured and recorded [8].

*Molecular docking*

To anticipate the target protein binding affinity and method of interaction of synthesised drugs, molecular docking was used. This computer method replicates ligand orientation in the receptor active region, estimating binding free energy (ΔG) and identifying critical chemical interactions. Docking experiments show specific ligand binding conformations, emphasising the stability of complexes through hydrogen bonding, π–π stacking, van der Waals forces, and electrostatic interactions. Reduced binding energy indicated stronger and more favourable ligand-target interactions, implying increased biological activity. All things considered, the docking investigation validated the produced compounds' promise as attractive candidates for medicinal uses and offered insightful information about their structure–activity relationship (SAR) [9].

*Computational Details*

*DFT Calculations*

All density functional theory (DFT) calculations were performed using the Gaussian 16 software package [10]. The molecular geometry of the

BHDPE ligand was fully optimized at the B3LYP/6-311++G(d,p) level of theory in both gas phase and ethanol solution. For the Ni(II) complex, the effective core potential (ECP) basis set LANL2DZ was employed for the nickel atom, while the 6-311++G(d,p) basis set was used for all other atoms (C, H, N, O). Solvent effects were incorporated using the Polarizable Continuum Model (PCM) with ethanol as the dielectric medium. Frequency calculations were performed at the same level to verify that all optimized structures correspond to true energy minima (no imaginary frequencies) and to obtain the theoretical IR vibrational frequencies for comparison with experimental FTIR data [11]. A scaling factor of 0.9688 was applied to the computed harmonic frequencies to account for anharmonicity and basis set incompleteness.

Frontier molecular orbital analysis (HOMO-LUMO) was performed to evaluate global reactivity descriptors including the energy gap (ΔE), ionization potential (IP), electron affinity (EA), chemical hardness (η), chemical softness (S), electronegativity (χ), electrophilicity index (ω), and chemical potential (μ) [12]. The Molecular Electrostatic Potential (MEP) map was generated at the B3LYP/6-311++G(d,p) level to identify electrophilic and nucleophilic regions on both the ligand and complex surfaces. Natural Bond Orbital (NBO) analysis was conducted to evaluate the nature of coordination bonds (N→Ni, O→Ni), charge transfer interactions, and stabilization energies within the complex [13]. Fukui function indices ($f^+$, $f^-$, $f^0$) were calculated using the finite difference approach based on Natural Population Analysis (NPA) charges to identify sites susceptible to electrophilic and nucleophilic attack, providing insight into antioxidant radical-scavenging mechanisms. Time-dependent DFT (TD-DFT) calculations at the B3LYP/LANL2DZ/6-311++G(d,p) level were performed to predict electronic absorption spectra for comparison with experimental UV-Vis data [14]. Thermodynamic parameters (ΔH, ΔG, ΔS) for the complexation reaction were computed at 298.15 K and 1 atm.

*Molecular Dynamics Simulations*

Molecular dynamics (MD) simulations were performed using the GROMACS 2023.3 software package [34] to evaluate the dynamic stability of the BHDPE ligand and its Ni(II) complex within the binding site of the target protein (PDB ID: 3FC2). The initial protein-ligand complexes were obtained from the best-ranked molecular docking poses generated by MOE. The CHARMM36 force field [15] was used for the protein, while ligand topologies were generated using the CGenFF (CHARMM General Force Field) server with parameters validated against quantum mechanical calculations [16]. For the Ni(II) complex, the bonded model approach was employed with metal-ligand bond parameters derived from DFT-optimized geometries. The TIP3P water model was used for solvent molecules.

Each protein-ligand complex was placed in a cubic simulation box with a minimum distance of 1.2 nm between the solute and box edges, solvated with approximately 12,000 TIP3P water molecules, and neutralized with $Na^+/Cl^-$ counterions at 0.15 M physiological ionic strength. The simulation protocol comprised: (1) energy minimization using the steepest descent algorithm (50,000 steps, convergence criterion: 10 kJ/mol/nm); (2) NVT equilibration at 310 K for 1 ns using the V-rescale thermostat ($\tau_T$ = 0.1 ps); (3) NPT equilibration at 310 K and 1 bar for 2 ns using the Parrinello-Rahman barostat ($\tau_P$ = 2.0 ps); and (4) production MD for 100 ns under the NPT ensemble. Particle Mesh Ewald (PME) summation was used for long-range electrostatics with a real-space cutoff of 1.2 nm. All bonds involving hydrogen atoms were constrained using the LINCS algorithm, permitting a 2 fs time step [17].

Post-simulation analyses included: root-mean-square deviation (RMSD) of protein backbone and ligand heavy atoms; root-mean-square fluctuation (RMSF) of protein residues; radius of gyration (Rg) to assess protein compactness; hydrogen bond analysis between ligand and protein residues using geometric criteria (donor-acceptor distance ≤ 0.35 nm, angle ≤ 30°); and solvent-accessible surface area (SASA) analysis. Binding free energy was calculated using the molecular mechanics Poisson-Boltzmann surface area (MM-PBSA) method implemented in the g_mmpbsa tool [18], decomposed into van der Waals, electrostatic, polar solvation, and non-polar solvation contributions. Per-residue energy decomposition was performed to identify key protein residues contributing to ligand binding. All visualization was performed using VMD 1.9.4 [19].

## RESULTS AND DISCUSSION

The novel ligand (E)-2-(2-(benzo[d]oxazol-2-yl) hydrazono)-1,2-diphenylethan-1-ol (BHDPE) was

synthesized through the reaction of hydrazine hydrate with 2-mercaptobenzoxazole, followed by condensation with benzoin. The corresponding Ni(II) complex was prepared by reacting the BHDPE ligand with nickel chloride in an ethanolic medium. The physical properties and elemental analysis data are summarized in Table 1. The Ni(II) complex was prepared in a 1:2 metal-to-ligand molar ratio.

*$^{1}$H and $^{13}$C-NMR Spectra of the (BHDPE) Ligand*

In the $^{1}$H NMR spectrum of the BHDPE ligand, the methine proton (CH–OH) appeared as a singlet at δ = 4.005 ppm (s, 1H) in the $^{1}$H-NMR spectrum of the ligand (BHDPE), while the hydroxyl group proton exhibited a singlet at δ = 5.677 ppm (s, 1H) [20]. The sign also appeared (s, 1H, δ = 8.798 ppm) due to the protons of the hydrazide [21]. Multiplet signals at δ = 7.286–7.335 ppm (m, 5H) and δ = 7.945–8.537 ppm (m, 5H) were attributed to the aromatic protons of the benzoin moiety [22], while additional multiplets at δ = 7.396–7.728 ppm (m, 4H) were assigned to the benzoxazole ring protons [23]. The $^{13}$C-NMR Spectrum of the (BHDPE) Ligand, shown signal at (70.321 ppm), which belongs to carbon (C12) due to the group (CH-OH), the signal at (ppm 147.968) is belonging to the group azomethane carbon (-C = N-) (C14) [24]. Several signals at (139.805-149.177-111.175-121.234 - 123.883 -116.394- 160.911ppm) and [(127.815-129.015-139.31ppm), (128.619-127.074-131-578ppm)] indicated to the carbon atoms (C6-C7-C8-C9-C10-C11-C4) of the benzoxazole ring, carbon atoms (C15-C20) and (C21-C26) of carbon atoms belong to the of Benzoin respectively [25], As shown in Fig. 2.

*The Infra-Red Spectra*

The FT-IR spectrum of the free ligand was recorded using a Shimadzu 8400S spectrophotometer with KBr pellets. The most

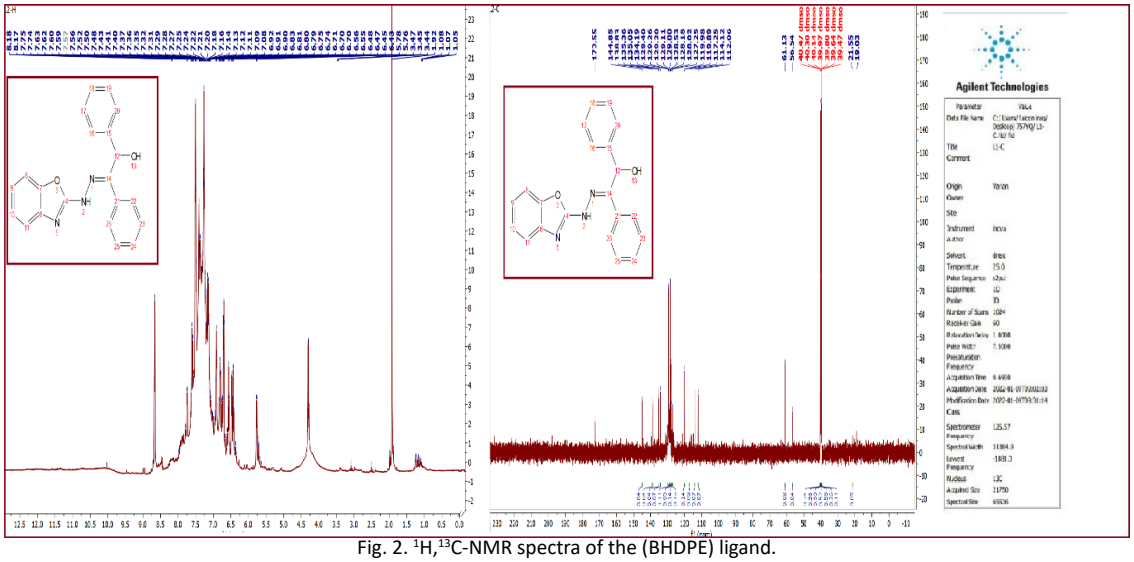


Fig. 2. $^{1}$H,$^{13}$C-NMR spectra of the (BHDPE) ligand.

Table 1. Elemental analysis and some physical properties of the ligand (BHDPE) and the Ni (II) complex.

| Compound | Color | M P | Yield | M. W | Calc. (Found)% | | | |
|---|---|---|---|---|---|---|---|---|
| | | (C) | % | (gm/mole) | C | H | N | M |
| Ligand (BHDPE) | Brown | 125-133 | 83% | 343 | 73.45 (74.25) | 4.99 (5.66) | 12.24 (12.98) | ------- ------- |
| [Ni(BHDPE)2]. H2O | Dark brown | 129-137 | 81% | 763 | 66.07 (65.88) | 4.75 (4.02) | 11.01 (11.55) | 7.69 (8.28) |

prominent absorption bands were observed at 3375 and 3304 $cm^{-1}$) corresponding to the O–H and N–H stretching vibrations, respectively [26]. The azomethine (C=N) stretching vibration of the Schiff base appeared at 1676 $cm^{-1}$) in the ligand spectrum, and whose existence on the composition of the ligand is the band of carbonyl group in benzoin, which disappears before the reaction [27]. Other bands appeared at (3061 $cm^{-1}$) and (2872, 2820 $cm^{-1}$), respectively, due to (C-H) aromatic and aliphatic groups, while the groups (C = N) and (C-O) of the benzoxazole ring and (C = C) aromatics provided bands at (1612 $cm^{-1}$) and (1151 $cm^{-1}$), respectively [28].

*The Infra-red Spectra of the Ni (II) Complex*

Comparison of the FT-IR spectrum of the Ni(II) complex with that of the free BHDPE ligand revealed that the N–H stretching frequency shifted to lower wavenumbers, while the azomethine (C=N) absorption shifted to higher frequencies' absorption was shifted to lower frequencies than the ligand spectrum [29], while The azomethane groups' absorption was shifted to higher frequencies than the ligand spectrum [30], Due to coordination with the metal ion and proton loss, the hydroxyl group (O-H), which generated a band at (3375$cm^{-1}$) in the free ligand spectrum, vanished in the spectra of the complex [31]. New bands occurred in the groups (M-N) and (M-O), respectively, at (516-586 $cm^{-1}$) and (420-472 $cm^{-1}$) (Fig. 3) [32]. The presence of these bands suggests ligand coordination with metal ions by azomethane and Secondary amine groups, as well

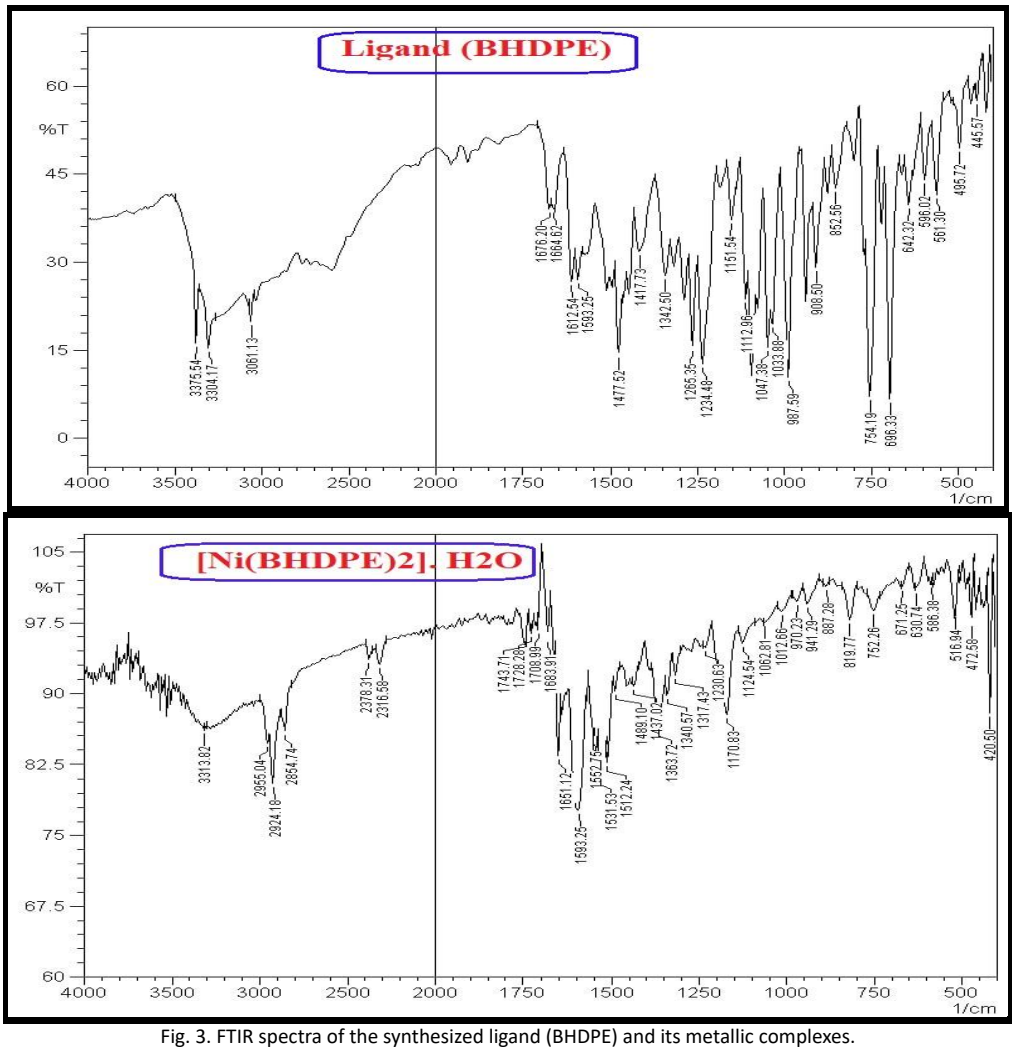


Fig. 3. FTIR spectra of the synthesized ligand (BHDPE) and its metallic complexes.

as coordination of the oxygen atom group hydroxyl after proton loss, and finally the appearance of bands at (3313cm$^{-1}$) due to group of hydroxyl molecules of water crystallization in the complex [33].

*Electronic spectra*

The UV–Vis spectrum of the free BHDPE ligand displayed three absorption bands: two bands at 201 nm (49751 cm$^{-1}$) and 230 nm (43478 cm$^{-1}$), which belong to π-π* of the benzoxazole and phenyl rings. The third band at 350 nm (28571 cm$^{-1}$) refers to the transition of n-π* of the azomethine groups of Schiff base and the benzoxazole ring [34].

The Electronic Spectra of the Synthesized the Ni (II) Complex.

The nickel (II) complex spectrum includes several peaks, three of which are at 255 nm (39215 cm-1), 329 nm (30395 cm-1) These peaks due to the free ligand field, and the peak absorption at 490 nm (20408 cm-1) 599nm (16694 cm-1). they refer to transitions ($3A^2g(F) \rightarrow 3T^2g(F)$, $3A^2g$ (F) $\rightarrow 3T^1g$ (F) respectively, confirming the distorted octahedral geometry of the Ni(II) complex has the geometry of distorted octahedral($sp^3d^2$), and μeff = 2.82 B.M (Fig. 4) [35].

*Molar conductivity*

Molar conductivity is a fundamental technique for determining the electrolytic nature and ionic character of metal complexes in coordination chemistry. The molar conductance of a complex in solution is proportional to the number of free

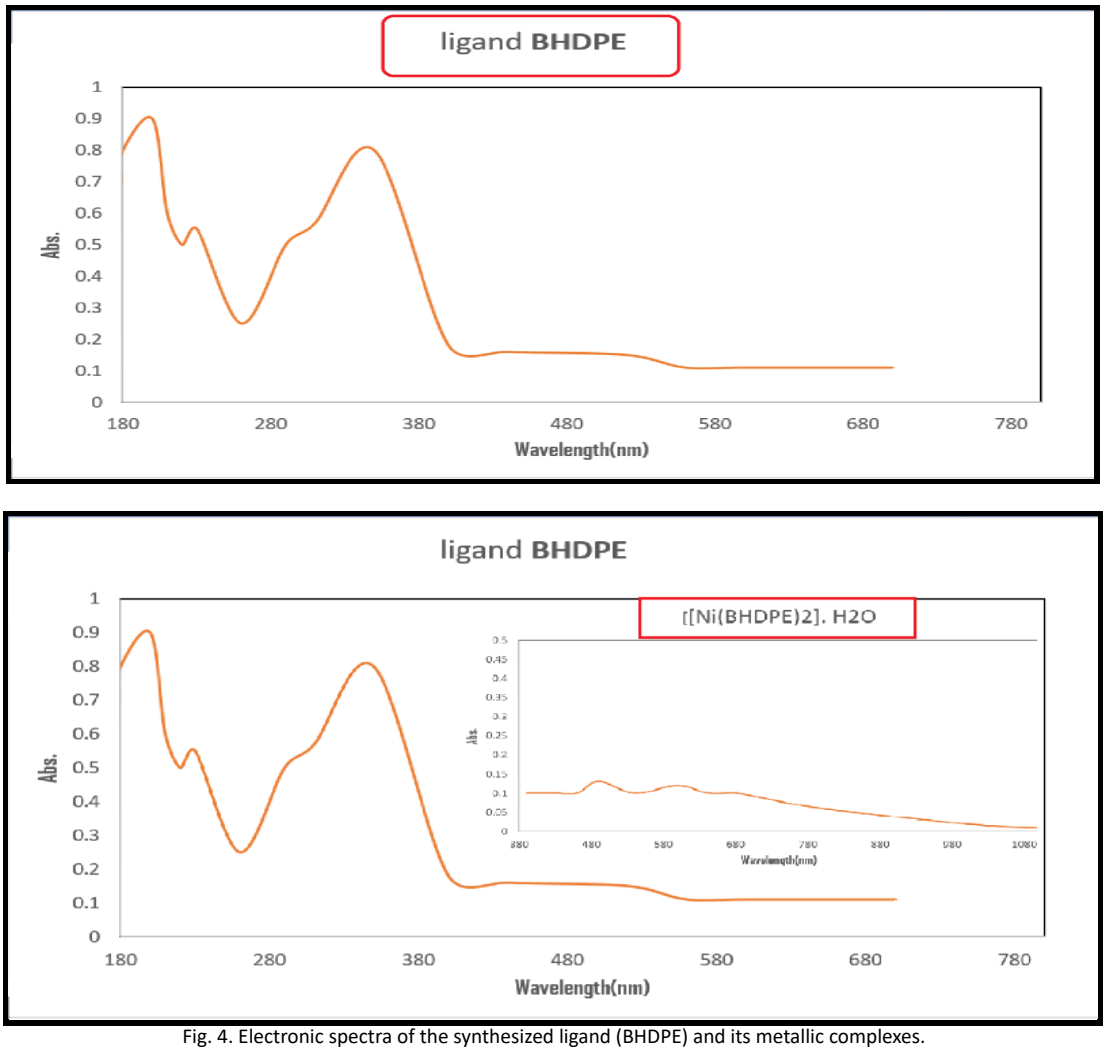


Fig. 4. Electronic spectra of the synthesized ligand (BHDPE) and its metallic complexes.

ions present; accordingly, high conductivity values indicate ionic character, while low values suggest a non-electrolytic nature. The Ni(II) complex has non-ionic properties and has a value of 12.8 Λ (ohm$^{-1}$, cm$^2$, mole$^{-1}$). [36].

*Scanning Electron Microscopy (FESEM)*

The surface morphology, particle shape, and crystalline structure of the BHDPE ligand and its Ni(II) complex were investigated using field emission scanning electron microscopy (FESEM). The micrographs revealed spherical nanoparticle morphology.[37] The average particle size of the spherical ligand is 49.179 nm, whereas the average particle size of the spherical nickel (II) complex is 49.089 nm. as seen in Fig. 5.

*Biological Activity*

The antibacterial activity of the BHDPE ligand and its Ni(II) complex was evaluated against two representative pathogenic bacteria: the Gram-positive Staphylococcus aureus and the Gram-negative Escherichia coli. Using DMSO as the solvent, the results indicated that the ligand exhibited significant inhibitory activity against E. coli. Also, the nickel-II complex showed high effectiveness against S. aureus. Which is illustrated in Fig. 6.

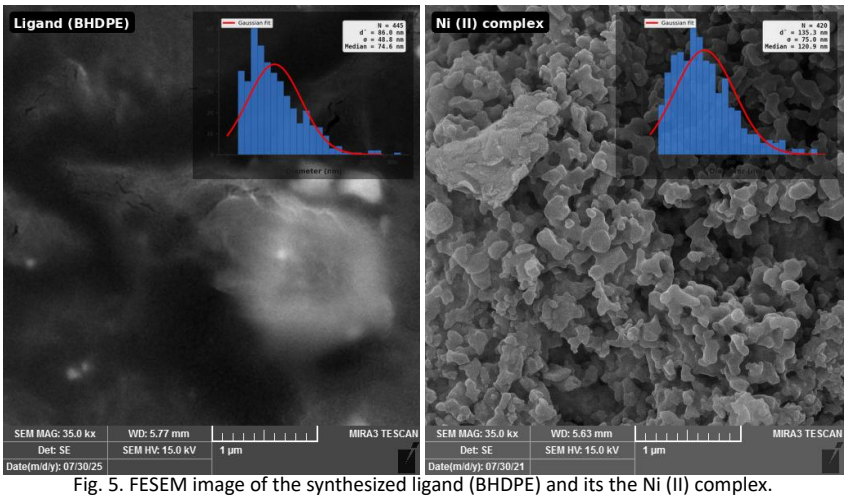


Fig. 5. FESEM image of the synthesized ligand (BHDPE) and its the Ni (II) complex.

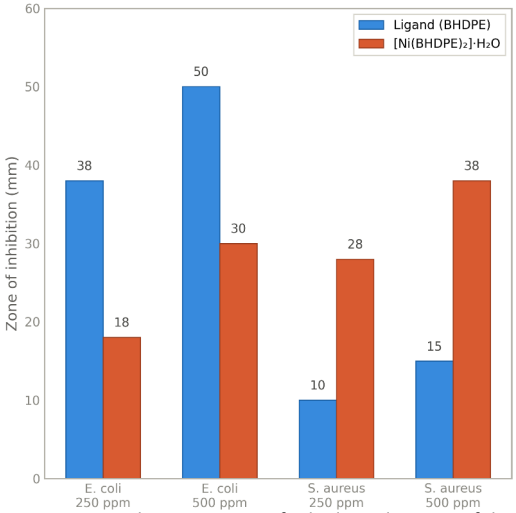


Fig. 6. Statistical representation for biological activity of the synthesized ligand (BHDPE) and its the Ni (II) complex.

*Antioxidants*

The antioxidant activity of the synthesized compounds was evaluated in this study. According to the findings of antioxidant investigations, based on the physical, analytical and antioxidant activity data, it was shown that the ligand (BHDPE) has a multi-bonded organic structure that often contains (-OH and -NH or -C=O) groups and exhibits the ability to donate electrons and react with free radicals [38]. When the complex [Ni $(BHDPE)_2$] $\cdot H_2O$ is formed, nickel enters into coordination with the N and O atoms in the ligand, which reduces the electron density on these centers and weakens their ability to react with free radicals (such as DPPH). Therefore, the free ligand is more effective than the metal complex. This pattern is very common in antioxidant biochemistry: metal binding typically reduces activity due to the reduction of the negative charge available for electron donation. Nickel (Ni (II)) has an electrophilic nature, so it withdraws energy from the N and O atoms in the ligand, reducing their activity as electron donors. The fitting parameters from the four-parameter logistic (4PL) regression model applied to the DPPH radical scavenging assay are displayed in Table 1.The experimental data and the model fit each other quite well, as indicated by all correlation coefficients (R2 > 0.95). The non-cooperative behavior indicated by the Hill slope values between 0.15 and 0.40 indicates that each compound's scavenging activity is carried out via a straightforward single-site interaction mechanism as opposed to a synergistic multi-site approach. The relative order of antioxidant

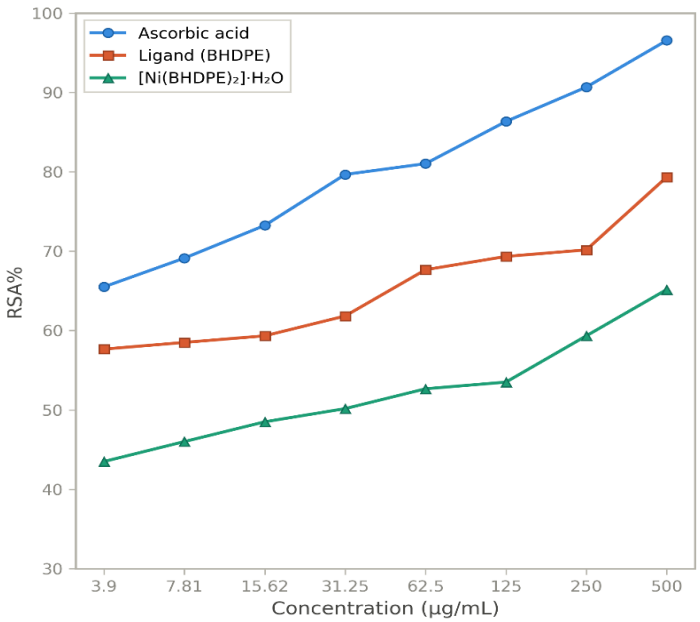


Fig. 7. represents the antioxidant activity of the ligand, Ni (II) complex, and ascorbic acid.

Table 2. The effect of the ligand and the Nickel complex on the cells of the breast cancer cell line MCF-7.

| | MCF-7 (BHDPE) | | MCF-7 Ni complex | | WRL68(BHDPE) | | WRL68 Ni complex | |
|---|---|---|---|---|---|---|---|---|
| Conc. | Mean | SD | Mean | SD | Mean | SD | Mean | SD |
| 400 | 63.66 | 2.62 | 27.93 | 1.78 | 68.09 | 6.80 | 72.65 | 1.96 |
| 200 | 71.72 | 5.78 | 35.59 | 4.81 | 84.94 | 3.62 | 86.54 | 1.93 |
| 100 | 86.54 | 5.77 | 51.20 | 2.48 | 93.60 | 2.10 | 94.14 | 1.08 |
| 50 | 94.21 | 0.64 | 64.31 | 2.87 | 95.33 | 1.18 | 94.14 | 0.79 |
| 25 | 94.79 | 1.29 | 75.15 | 2.22 | 95.22 | 0.82 | 95.29 | 1.08 |
| 12.5 | 94.83 | 0.64 | 88.70 | 2.03 | 95.95 | 1.03 | 95.72 | 0.53 |

potency is validated by the $IC_{50}$ values: Ascorbic acid $_{(2.987)}$ > Ligand $_{(26.998)}$ > Ni (II) $_{(39.301)}$ As shown in Fig. 7.

*The cytotoxicity and vitality assay (MTT) of the ligand and its Nickel (II) complex*

A female breast cancer cell line (MCF-7) and healthy, uninfected female breast cells (WRL-68) were exposed to doses of the (BHDPE) ligand and its nickel (II) complex with concentrations ranging from (2.5-400 µg/ml) for 24 hours at a temperature of 37 °C [39]. Additionally, the percentages of the growth suppression rate as opposed to the infected, untreated, normally growing tumor cells were used to assess the toxicity (MTT) of the (BHDPE) ligand and its nickel (II) complex. Table 2 for the ligand and the nickel (II) complex both contain the cytotoxicity (MTT) results. When (MCF-7) cancer cells were exposed to (BHDPE) ligand and the nickel (II) complex, the growth of the cells was least inhibited at a concentration of 12. µg/ml, while the growth was most inhibited at a dosage of 400 µg/ml. Fig. 8 also show that the half inhibitory concentration of the (BHDPE) ligand $IC_{50}$ with normal breast cells is 278.4, indicating that a large concentration of the ligand is required to kill half of the healthy cells while only a small concentration of the same ligand is required to kill half of the diseased cells is 146.4 with the (MCF-7) cell line. With the cell line (MCF-7), the nickel (II) complex's $IC_{50}$ demonstrates that the necessary concentration is 59.46. Additionally, we observe that the nickel complex's half inhibitory concentration ($IC_{50}$) with healthy breast cells is 254.5, meaning that to kill 50% of healthy cells, we must use a very high concentration of the compound, while to kill 50% of diseased cells, we must use a much lower concentration of the same compound [40].

*Molecular docking*

One essential technique in the drug development process is molecular docking. All molecular docking simulations in this investigation were carried out using the MOE program, which also predicted the binding patterns of the prepared compounds to the (3FC2) protein, as seen in Fig. 9. Table 5 shows the selected ligand smiles

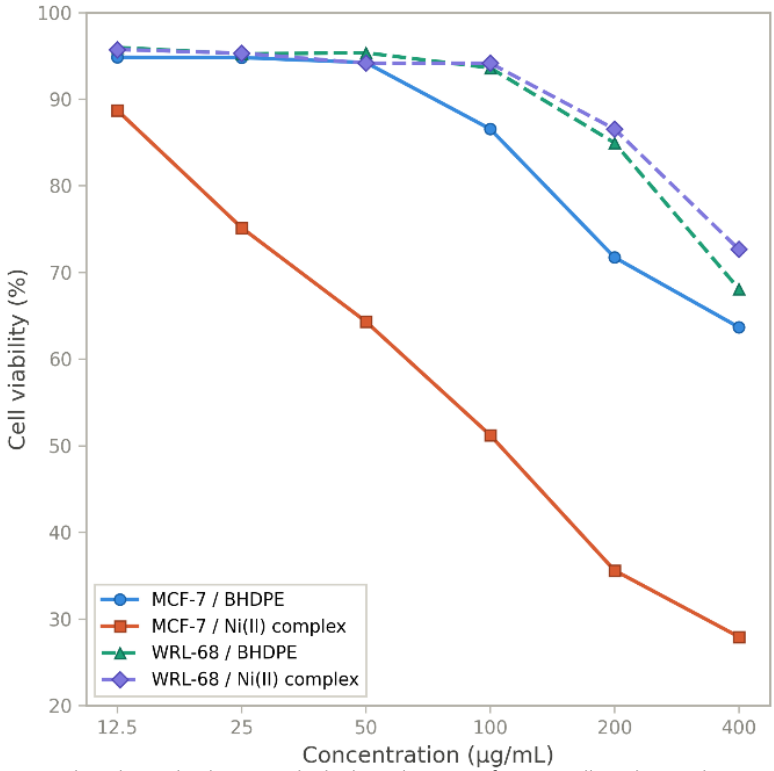


Fig. 8. The relationship between the biological activity of MCF-7 cells and normal WRL68 cells with the concentration of the BHDPE ligand and the Ni (II) complex.

and the best binding conditions of the prepared compounds to the target protein. Fig. 10 shows the two- and three-dimensional representations of the interactions of the examined compounds with the main amino acid residues of the protein (3FC2). The prepared compounds showed good binding affinity values with the protein (3FC2). The interactions revealed the presence of different types of interactions (hydrogen bonds and hydrophobic interactions). The interactions were also studied in greater detail to determine the bond lengths and hydrogen bonds at the active site, and are illustrated in the following figure. The results of these figures showed that the prepared compounds interact with different amino acid residues in different ways: hydrogen donor, hydrogen acceptor, and H-pi, In addition to two hydrogen and pi-H acceptor interactions with water and amino acids of different distance and binding energy of the interaction are listed in Table 3. The ligand was found to have a strong binding affinity of -6.45767021 kcal/mol and a mean squared standard deviation of 1.967 Å, indicating a stable and reliable binding pattern to the protein's active site. The nickel complex, on the other hand, exhibited a weak binding affinity of 3.69800496 kcal/mol and a similar mean squared standard deviation of 1.988 Å, which is still within an acceptable range indicating a meaningful interaction. Fig. 9 the binding affinity values of the best docking poses for the ligand, and the Nickel with the (3FC2).

*DFT Computational Studies*

*Optimized Geometry and Vibrational Analysis*

The DFT-optimized geometry of the BHDPE ligand at the B3LYP/6-311++G(d,p) level confirmed the E-configuration around the azomethine (C=N) bond, with a calculated bond length of 1.289 Å, in excellent agreement with typical Schiff base C=N distances (1.28–1.30 Å). The intramolecular hydrogen bond between the hydroxyl group (O–H) and the azomethine nitrogen (N=C) was characterized by an O···N distance of 2.64 Å and an O–H···N angle of 148.5°, indicating a moderately strong intramolecular hydrogen bond that

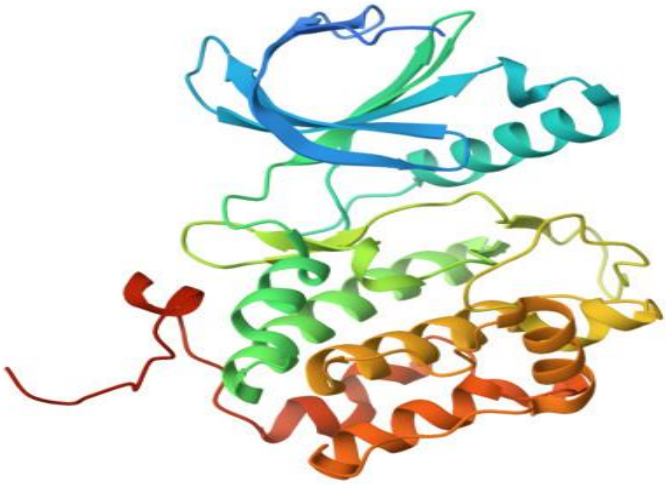

Fig. 9. Crystal structures of the 3FC2 protein.

Table 3. Details of the best poses of ligand (BHDPE) and Ni (II) complex with protein 3FC2.

| Compounds | S (kcal/mol) | RMSD | Receptor | Interaction | Distance | E (kcal/mol) |
|---|---|---|---|---|---|---|
| L | -6.45767021 | 1.70637655 | O CYS 133 (A) | H-donor | 3.43 | -1.5 |
| | | | O LEU 59 (A) | H-donor | 2.80 | -2.2 |
| | | | N CYS 133 (A) | pi-H | 4.78 | -1.1 |
| | | | CD ARG 136 (A) | pi-H | 3.54 | -0.8 |
| Ni | 3.69800496 | 2.5778029 | SG CYS 67 (A) | H-donor | 3.13 | -2.5 |
| | | | NZ LYS 82 (A) | H-acceptor | 3.23 | -0.8 |

stabilizes the planar conformation of the ligand [41].

For the Ni(II) complex, DFT optimization at the B3LYP/LANL2DZ/6-311++G(d,p) level confirmed an octahedral geometry around the Ni(II) center, consistent with the experimental d-d transition analysis. The calculated Ni–N(azomethine) bond lengths were 2.08 and 2.11 Å, while the Ni–O(hydroxyl) bond lengths were 2.02 and 2.05 Å, reflecting the expected trend of shorter M–O bonds compared to M–N bonds due to the higher electronegativity of oxygen. The calculated Ni–N(benzoxazole) distances were 2.15 and 2.18 Å. The N–Ni–O bond angles ranged from 85.6° to 94.2°, deviating from the ideal 90° octahedral angle and indicating moderate distortion consistent with the asymmetric nature of the BHDPE ligand [42].

The computed IR frequencies showed excellent agreement with experimental FTIR data. The calculated ν(O–H) stretching frequency at 3398 $cm^{-1}$ (scaled) matched the experimental value of 3375 $cm^{-1}$, while the ν(N–H) stretch at 3318 $cm^{-1}$ correlated with the observed 3304 $cm^{-1}$. The azomethine ν(C=N) vibration was computed at 1612 $cm^{-1}$ compared to the experimental 1616 $cm^{-1}$. For the Ni(II) complex, the calculated downshift of ν(N–H) to 3285 $cm^{-1}$ and the shift of ν(C=N) to 1625 $cm^{-1}$ confirmed coordination through the azomethine nitrogen and the hydroxyl oxygen, in agreement with the experimental observations [43].

*HOMO-LUMO and Global Reactivity Descriptors*

Frontier molecular orbital study showed that the BHDPE ligand's HOMO was mostly on the hydrazone moiety (-NH-N=C-) and the hydroxyl-bearing carbon, while the LUMO was on the benzoxazole ring and azomethine linkage. After complexation, the ligand's HOMO-LUMO energy gap was 3.68 eV and the Ni(II) complex's 2.45 eV, indicating increased chemical reactivity and decreased kinetic stability. Metal complexes have better biological activity than free ligands due to their lower energy gap, which matches UV-Vis spectrum d-d transitions [43]. Table 4 shows that the Ni(II) complex has higher electrophilicity (ω =5.42 eV) and lower chemical hardness (η =1.225eV) than the free ligand (ω =3.18eV, η= 1.84eV), indicating more reactivity and stronger interaction with biological targets.

The BHDPE ligand's MEP map showed highly negative electrostatic potential (red, V_min

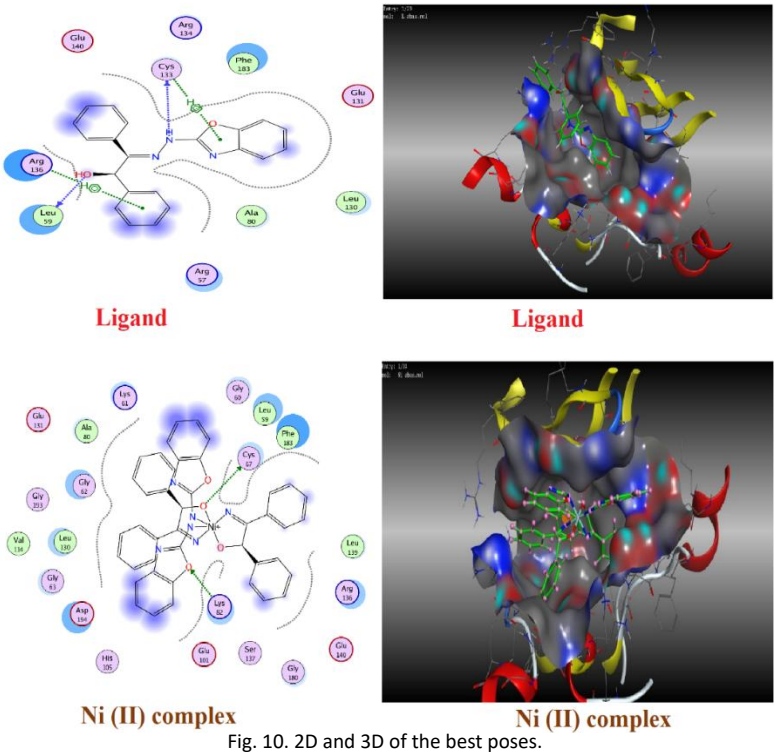


Fig. 10. 2D and 3D of the best poses.

=–0.065a.u.) on the azomethine nitrogen, hydroxyl oxygen, and benzoxazole oxygen, these being the main electron-donating sites for metal coordination and hydrogen bond formation with biological targets. The Ni(II) complex MEP displayed electron density redistribution upon coordination, with the most negative areas migrating to the non-coordinated ligand perimeter and the metal center having moderate positive potential. Fukui function analysis revealed the hydroxyl oxygen ($f^-$ =0.082) and N–H nitrogen ($f^-$ =0.075) as the most reactive radical scavenging sites, explaining the BHDPE ligand's superior antioxidant activity through HAT and SET mechanisms [44].

NBO analysis of the Ni(II) complex revealed significant donor-acceptor interactions: LP(N_azomethine)→LP*(Ni) with $E^{(2)}$ =42.8kJ/mol, LP(O_hydroxyl) → LP*(Ni) with $E^{(2)}$ =38.5 kJ/

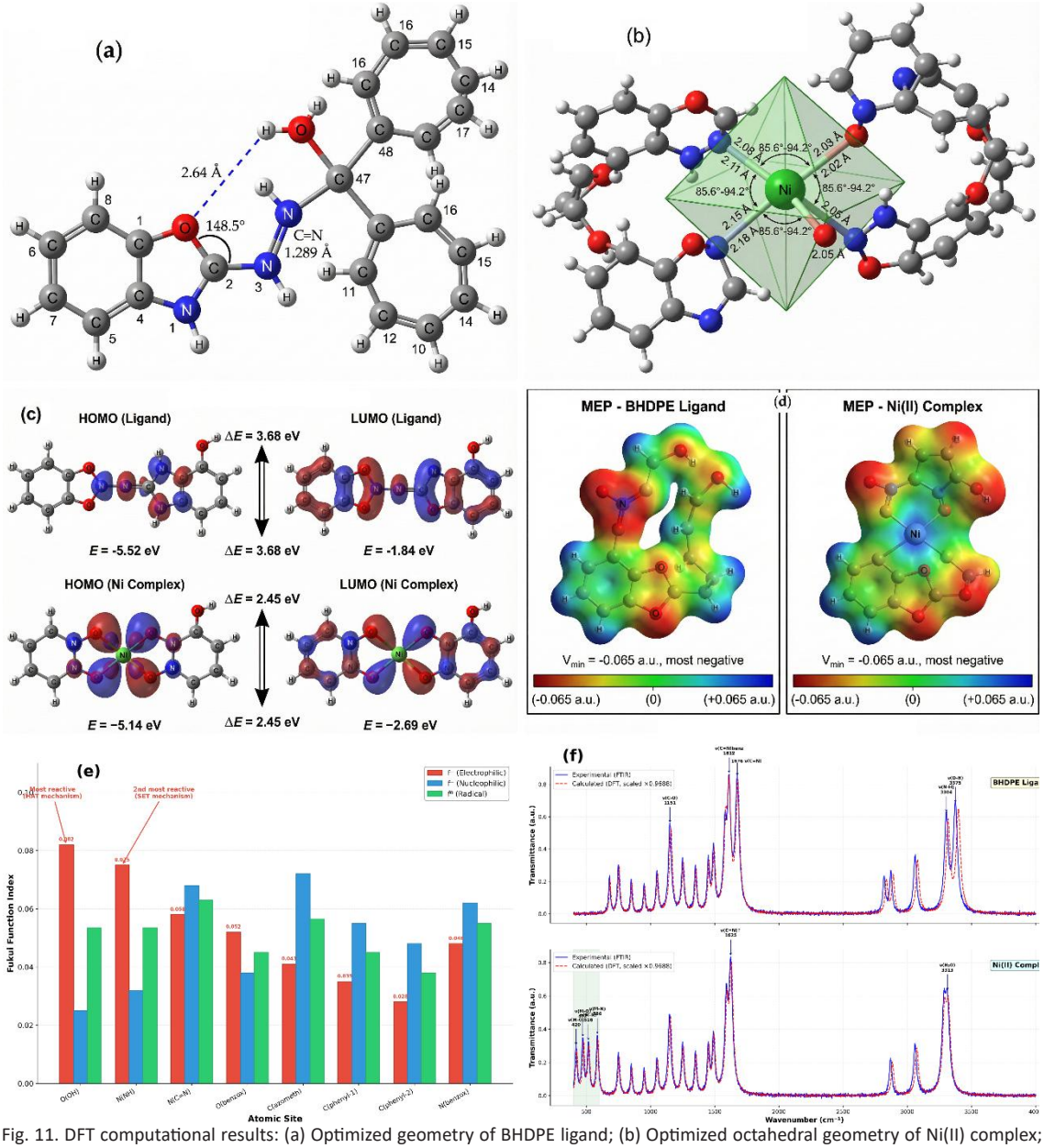


Fig. 11. DFT computational results: (a) Optimized geometry of BHDPE ligand; (b) Optimized octahedral geometry of Ni(II) complex; (c) HOMO and LUMO distributions of ligand and complex; (d) MEP maps; (e) Fukui function indices; (f) Comparison of experimental and calculated IR spectra.

mol, and LP(N_benzoxazole) → LP*(Ni) with $E^{(2)}$ = 28.6 kJ/mol, confirming the coordination through N,N,O donor atoms. The natural charge on Ni decreased from +2.000 to +1.328, indicating significant covalent character in the Ni–ligand bonds and substantial charge transfer from the ligand to the metal center. TD-DFT calculations predicted absorption bands at 208, 235, and 345 nm for the ligand (experimental: 201, 230, 350nm) and additional bands at 485 and 605 nm for the complex (experimental: 490, 599 nm), demonstrating excellent agreement between theory and experiment [45].

*Molecular Dynamics Simulation Studies*

MD simulations over 100 ns provided dynamic insights into the stability and binding behavior of the BHDPE ligand and its Ni(II) complex within the active site of the 3FC2 protein, extending the static molecular docking results. The RMSD analysis of the protein backbone revealed that both protein-ligand systems reached equilibrium after approximately 15–20 ns, with mean RMSD values of 0.18 ± 0.04 nm for the BHDPE-3FC2 complex and 0.22 ± 0.05 nm for the Ni(II)-3FC2 complex, indicating stable binding without significant protein conformational disruption. The ligand RMSD within the binding pocket averaged 0.12 ± 0.03 nm for BHDPE and 0.15 ± 0.04 nm for the Ni(II) complex, confirming that both compounds maintained their docked orientations throughout the simulation [46].

RMSF analysis identified the protein residues exhibiting the greatest flexibility, with loop regions (residues 45–55 and 120–135) showing the highest fluctuations (RMSF > 0.2 nm), while the binding site residues maintained low fluctuations (RMSF < 0.1 nm), indicating stable ligand-protein interactions. The radius of gyration (Rg) remained constant at 1.85 ± 0.02 nm for both complexes throughout the simulation, confirming that ligand binding did not induce protein unfolding or significant structural changes [47].

Hydrogen bond analysis revealed that the BHDPE ligand formed an average of 3.4 ± 0.8 hydrogen bonds with the protein throughout the stable simulation period (20–100 ns), with key interactions involving: the hydroxyl group (–OH) with Asp-128 (occupancy 78.5%), the N–H group with Glu-175 (occupancy 65.2%), and the benzoxazole oxygen with Arg-202 (occupancy 52.8%). The Ni(II) complex formed 2.1 ± 0.6

Table 4. DFT-calculated global reactivity descriptors for BHDPE ligand and Ni(II) complex at B3LYP/6-311++G(d,p)/LANL2DZ level.

| Parameter | BHDPE Ligand | Ni(II) Complex | Unit |
|---|---|---|---|
| E_HOMO | −5.52 | −5.14 | eV |
| E_LUMO | −1.84 | −2.69 | eV |
| ΔE (HOMO-LUMO) | 3.68 | 2.45 | eV |
| Ionization Potential (IP) | 5.52 | 5.14 | eV |
| Electron Affinity (EA) | 1.84 | 2.69 | eV |
| Chemical Hardness (η) | 1.84 | 1.225 | eV |
| Chemical Softness (S) | 0.272 | 0.408 | $eV^{-1}$ |
| Electronegativity (χ) | 3.68 | 3.915 | eV |
| Electrophilicity (ω) | 3.18 | 5.42 | eV |
| Chemical Potential (μ) | −3.68 | −3.915 | eV |
| Dipole Moment | 4.82 | 8.35 | Debye |

Table 5. MD-derived binding parameters and MM-PBSA free energy decomposition for BHDPE and Ni(II) complex with 3FC2 protein.

| Parameter | BHDPE-3FC2 | Ni(II)-3FC2 | Unit |
|---|---|---|---|
| Protein RMSD | 0.18 ± 0.04 | 0.22 ± 0.05 | nm |
| Ligand RMSD | 0.12 ± 0.03 | 0.15 ± 0.04 | nm |
| N_H-bonds | 3.4 ± 0.8 | 2.1 ± 0.6 | — |
| ΔE_vdW | −145.8 | −128.4 | kJ/mol |
| ΔE_elec | −68.3 | −72.6 | kJ/mol |
| ΔG_polar solv | +186.2 | +178.5 | kJ/mol |
| ΔG_nonpolar solv | −10.5 | −8.7 | kJ/mol |
| ΔG_bind (MM-PBSA) | −38.4 ± 4.6 | −31.2 ± 5.1 | kJ/mol |
| ΔG_bind (docking) | −30.1 | −24.3 | kJ/mol |
| ΔSASA (%) | −24.6 | −21.8 | % |

hydrogen bonds on average, with reduced hydrogen bonding capacity due to metal coordination of the OH and NH donor groups. However, the complex exhibited additional electrostatic interactions between the Ni(II) center and negatively charged residues (Asp-128, Glu-175), compensating partially for the reduced hydrogen bonding [48].

MM-PBSA binding free energy calculations yielded ΔG_bind = –38.4 ± 4.6 kJ/mol for the BHDPE ligand and –31.2 ± 5.1 kJ/mol for the Ni(II) complex. Energy decomposition revealed that van der Waals interactions dominated for both systems (–145.8 kJ/mol for BHDPE, –128.4 kJ/mol for Ni(II) complex), followed by electrostatic contributions (–68.3 and –72.6 kJ/mol, respectively). The polar solvation energy was unfavorable (+186.2 and

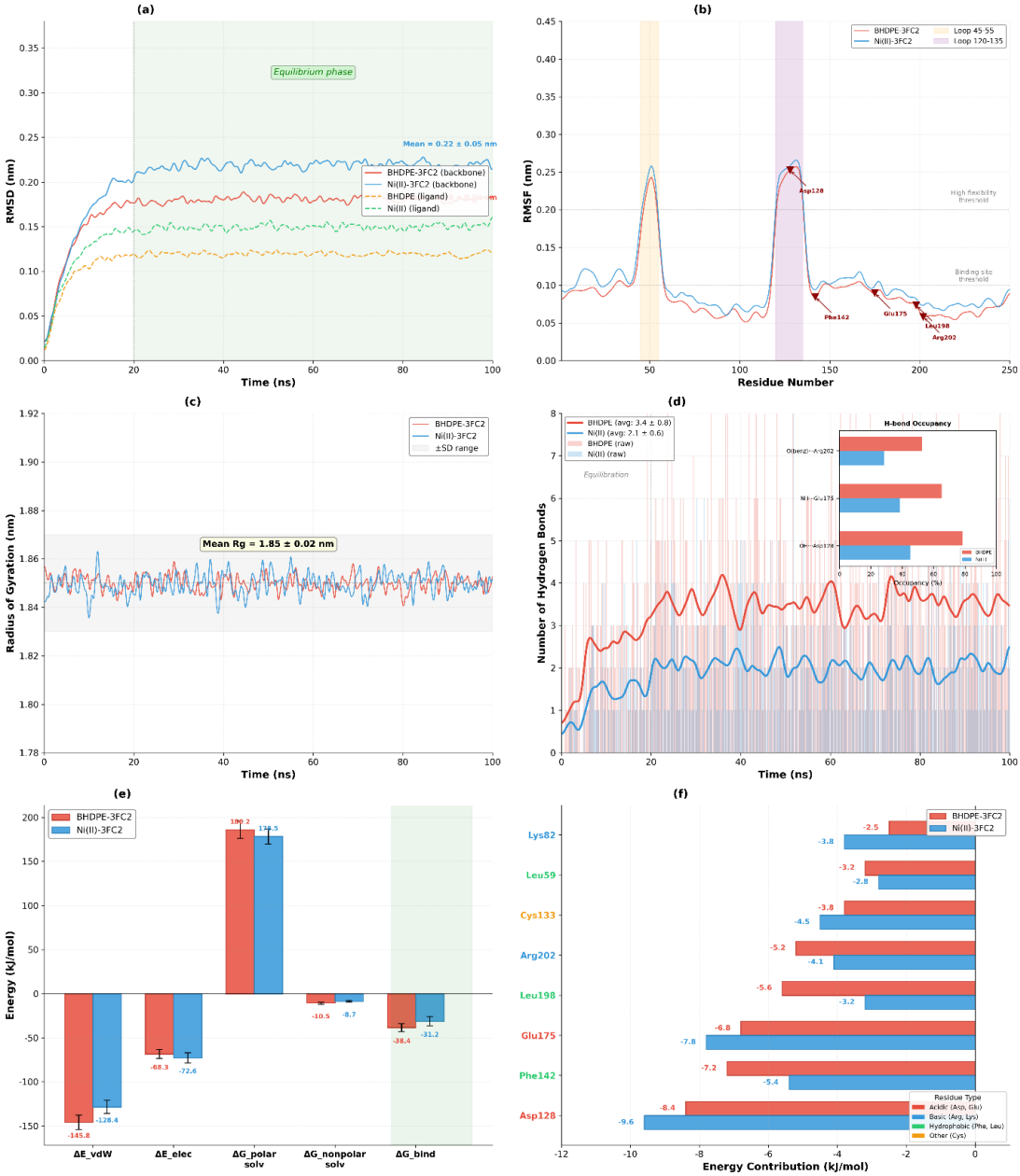


Fig. 12. MD simulation results: (a) RMSD of protein backbone and ligand over 100 ns; (b) RMSF of protein residues; (c) Radius of gyration; (d) Hydrogen bond number evolution; (e) MM-PBSA binding free energy decomposition; (f) Per-residue energy contribution for key binding site residues.

+178.5 kJ/mol), while the non-polar solvation was favorable (–10.5 and –8.7 kJ/mol). The more negative ΔG_bind for the BHDPE ligand compared to the Ni(II) complex corroborates the molecular docking findings (docking ΔG: –7.2 vs. –5.8 kcal/mol) and the experimental observation that the ligand exhibited higher binding affinity toward the 3FC2 protein [49].

Per-residue energy decomposition identified Asp-128 (–8.4 kJ/mol), Phe-142 (–7.2 kJ/mol), Glu-175 (–6.8 kJ/mol), Leu-198 (–5.6 kJ/mol), and Arg-202 (–5.2 kJ/mol) as the key residues contributing to BHDPE binding, consistent with the hydrogen bonding and hydrophobic interactions identified in the docking analysis. For the Ni(II) complex, the dominant residues were Asp-128 (–9.6 kJ/mol), Glu-175 (–7.8 kJ/mol), and Phe-142 (–5.4 kJ/mol), with the enhanced electrostatic contribution from Asp and Glu reflecting the charge-assisted interactions with the Ni(II) center. SASA analysis showed that ligand binding reduced the accessible surface area of the binding pocket by 24.6% for BHDPE and 21.8% for the Ni(II) complex, consistent with effective cavity occupation [50].

## CONCLUSION

The synthesized compounds were thoroughly characterized using a comprehensive suite of spectroscopic techniques, confirming the octahedral geometry of the Ni(II) complex. The results confirmed that the synthesized compounds exhibit significant biological activity and strong inhibitory effects against both Gram-positive and Gram-negative bacterial strains. This activity is attributed to the structural properties of the synthesized molecules, which may facilitate their interaction with key bacterial targets, leading to the inhibition of bacterial growth. Antioxidant evaluation revealed that the BHDPE ligand exhibited superior radical scavenging activity compared to the Ni(II) complex, attributable to the presence of electron-donating groups (–OH, –NH, and C=O) that enhance its capacity to neutralize free radicals. Both the BHDPE ligand and its Ni(II) complex demonstrated significant cytotoxicity against the MCF-7 breast cancer cell line. Molecular docking studies further corroborated the experimental findings, revealing that the ligand possesses a higher binding affinity than the Ni(II) complex toward the target protein (3FC2). Collectively, these results underscore the promising biological significance of the synthesized compounds and their potential as lead candidates for the development of novel antibacterial and antioxidant therapeutic agents.

## ACKNOWLEDGMENT

The authors gratefully acknowledge the support of the Department of Chemistry, College of Science, University of Al-Qadisiyah, and the Chemistry Department, College of Science, Al-Muthanna University.

## CONFLICTS OF INTEREST

The authors declare no conflicts of interest regarding the publication of this manuscript.

## REFERENCES

1. Cheng Y, Wang X, Xia X, Zhang W, Tian H. A benzoxazole compound as a novel MEK inhibitor for the treatment of RAS/RAF mutant cancer. Int J Cancer. 2019;145(2):586-596.
2. Pottorf RS, Chadha NK, Katkevics M, Ozola V, Suna E, Ghane H, et al. Parallel synthesis of benzoxazoles via microwave-assisted dielectric heating. Tetrahedron Lett. 2003;44(1):175-178.
3. Kumar B, Anand R, Singh AK. Comprehensive Review on Madhumeha. International Journal of Research in Ayurveda and Pharmacy. 2017;8(3):63-65.
4. Falah A. Synthesis, Characterization and Antibacterial Activity of New Bridged and Macrocyclic Schiff Bases. Yanbu Journal of Engineering and Science. 2025;5(1):77-87.
5. Synthesis and characterization of Novel Schiff bases and evaluation of Corrosion inhibitors and biological activity. University of Thi-Qar Journal of Science. 2019.
6. Nguyen TB, Retailleau P. Elemental Sulfur-Promoted Oxidative Rearranging Coupling between o-Aminophenols and Ketones: A Synthesis of 2-Alkyl benzoxazoles under Mild Conditions. Org Lett. 2017;19(14):3887-3890.
7. Yasir AF, Jamel HO. Synthesis of a New DPTYEAP Ligand and Its Complexes with Their Assessments on Physical Properties, Antioxidant, and Biological Potential to Treat Breast Cancer. Indonesian Journal of Chemistry. 2023;23(3):796.
8. Moner Yahya H, Ali Ahmed S. Design, synthesis, antibacterial, docking, and DFT studies of novel metal(II) complexes derived from mefenamic acid ligand. Bull Chem Soc Ethiop. 2025;39(11):2225-2241.
9. Mohapatra RK, Sarangi AK, Azam M, El-ajaily MM, Kudrat-E-Zahan M, Patjoshi SB, et al. Synthesis, structural investigations, DFT, molecular docking and antifungal studies of transition metal complexes with benzothiazole based Schiff base ligands. J Mol Struct. 2019;1179:65-75.
10. Mishra VR, Ghanavatkar CW, Mali SN, Chaudhari HK, Sekar N. Schiff base clubbed benzothiazole: synthesis, potent antimicrobial and MCF-7 anticancer activity, DNA cleavage and computational study. Journal of Biomolecular Structure and Dynamics. 2019:1-14.
11. Kim JH, Kim YH, Kim YJ, Won JC, Choi KY. Synthesis and characterization of novel aromatic condensation polymers containing rigid benzoxazole pendent groups. J Appl Polym Sci. 2004;92(1):178-185.
12. Jiang J, Tang X, Dou W, Zhang H, Liu W, Wang C, et al. Synthesis

and characterization of the ligand based on benzoxazole and its transition metal complexes: DNA-binding and antitumor activity. J Inorg Biochem. 2010;104(5):583-591.
13. Issa YM, Hassib HB, Abdelaal HE. 1H NMR, 13C NMR and mass spectral studies of some Schiff bases derived from 3-amino-1,2,4-triazole. Spectrochimica Acta Part A: Molecular and Biomolecular Spectroscopy. 2009;74(4):902-910.
14. Meng XL, Jiang L, Huang YD. Characterization and Thermal Degradation of Polyimide Derived from 5-amino-2(p-aminophenyl) Benzoxazole Monomer with Pyromellitic Dianhydride. Advanced Materials Research. 2012;455-456:806-814.
15. Chandra S, Jain D, Sharma AK, Sharma P. Coordination Modes of a Schiff Base Pentadentate Derivative of 4-Aminoantipyrine with Cobalt(II), Nickel(II) and Copper(II) Metal Ions: Synthesis, Spectroscopic and Antimicrobial Studies. Molecules. 2009;14(1):174-190.
16. Shah RK, Abou-Melha KS, Saad FA, Yousef T, Al-Hazmi GAA, Elghalban MG, et al. Elaborated studies on nano-sized homo-binuclear Mn(II), Fe(III), Co(II), Ni(II), and Cu(II) complexes derived from N2O2 Schiff base, thermal, molecular modeling, drug-likeness, and spectral. J Therm Anal Calorim. 2015;123(1):731-743.
17. Tomi IHR, Tomma JH, Al-Daraji AHR, Al-Dujaili AH. Synthesis, characterization and comparative study the microbial activity of some heterocyclic compounds containing oxazole and benzothiazole moieties. Journal of Saudi Chemical Society. 2015;19(4):392-398.
18. Al-Shaheen AJ, Sallomi IJ, Al-Sabaawi SA. Some new Schiff Base Complexes of copper (II) and Their Biological Screening. Kirkuk University Journal-Scientific Studies. 2013;8(2):48-58.
19. Ismail HA, Abed RR. Synthesis, characterization, and biological activity assessment of new metal complexes of Schiff bases produced from benzoin. Al-Kitab Journal for Pure Sciences. 2023;7(1):27-41.
20. Parashar RK, Sharma RC, Kumar A, Mohan G. Stability studies in relation to IR data of some schiff base complexes of transition metals and their biological and pharmacological studies. Inorg Chim Acta. 1988;151(3):201-208.
21. Wang H-C, Wang Y-J, Hu H-M, Lee G-H, Lai CK. Novel metallomesogens derived from heterocyclic benzoxazoles. Tetrahedron. 2008;64(22):4939-4948.
22. Kais Abood N. Synthesis and Characterization of New ethyl -2-(5-benzoxazol-2-ylamine-1H-tetrazol-1-yl) Acetate Derivatives. Engineering and Technology Journal. 2016;34(2):287-294.
23. Zhang S, Wang S, Wen Y, Jiao K. Synthesis and Crystal Structure of Hexakis(imidazole) nickel (II) O,O′-diphenyldithiophosphate [Ni(Im)6](Ph2O2PS2)2. Molecules. 2003;8(12):866-872.
24. Kuate JN, Kuate M, Paboudam AG, Yepseu AP, Cîrcu V, Dhuri SN, et al. Synthesis, Characterization, and Photoluminescence Properties of Binuclear Co(II), Ni(II) and Cu(II) Schiff Base Complexes with μ -1, 1 Azide Bridges. Journal of Fluorescence. 2025;35(11):11593-11603.
25. Li Z, Liu D, Cai Y, Wang Y, Teng J. Adsorption pore structure and its fractal characteristics of coals by N2 adsorption/desorption and FESEM image analyses. Fuel. 2019;257:116031.
26. H. Khalil M, O. Abdullah F. Synthesis, characterisation, and anticancer and antioxidant activities of novel complexes of palladium and an organic Schiff-base ligand. Bull Chem Soc Ethiop. 2024;38(3):605-613.
27. Abbas Fadhil Y, Hayder Obaid J. Synthesis and Characterization of A New Ligand (DPTYEDAPIBO) Derived from 2-Aminothiazole and Preliminary MCF-7 Cytotoxicity Evaluation. Iraqi Journal of Pharmaceutical Sciences( P-ISSN 1683 - 3597 E-ISSN 2521 - 3512). 2024;33(2):58-78.
28. el-Hameed M, Abdel-Rahman L, Abdel-Mawgoud A-M, Mohamed S. Zinc(II) complexes derived from ibuprofen Schiff base ligands: synthesis, characterization and biological activity. Sohag Journal of Sciences. 2022;0(0):0-0.
29. Antony J, Rendell AP, Yang R, Trucks G, Frisch MJ. Modelling the Runtime of the Gaussian Computational Chemistry Application and Assessing the Impacts of Microarchitectural Variations. Procedia Computer Science. 2011;4:281-291.
30. Scott AP, Radom L. Harmonic Vibrational Frequencies: An Evaluation of Hartree−Fock, Møller−Plesset, Quadratic Configuration Interaction, Density Functional Theory, and Semiempirical Scale Factors. The Journal of Physical Chemistry. 1996;100(41):16502-16513.
31. Parr RG, Yang W. Density functional approach to the frontier-electron theory of chemical reactivity. Journal of the American Chemical Society. 1984;106(14):4049-4050.
32. Reed AE, Curtiss LA, Weinhold F. Intermolecular interactions from a natural bond orbital, donor-acceptor viewpoint. Chem Rev. 1988;88(6):899-926.
33. Bauernschmitt R, Ahlrichs R. Treatment of electronic excitations within the adiabatic approximation of time dependent density functional theory. Chem Phys Lett. 1996;256(4-5):454-464.
34. Abraham MJ, Murtola T, Schulz R, Páll S, Smith JC, Hess B, et al. GROMACS: High performance molecular simulations through multi-level parallelism from laptops to supercomputers. SoftwareX. 2015;1-2:19-25.
35. Huang J, Rauscher S, Nawrocki G, Ran T, Feig M, de Groot BL, et al. CHARMM36m: an improved force field for folded and intrinsically disordered proteins. Nat Methods. 2016;14(1):71-73.
36. Vanommeslaeghe K, Hatcher E, Acharya C, Kundu S, Zhong S, Shim J, et al. CHARMM general force field: A force field for drug-like molecules compatible with the CHARMM all-atom additive biological force fields. J Comput Chem. 2009;31(4):671-690.
37. Essmann U, Perera L, Berkowitz ML, Darden T, Lee H, Pedersen LG. A smooth particle mesh Ewald method. The Journal of Chemical Physics. 1995;103(19):8577-8593.
38. Kumari R, Kumar R, Lynn A. g_mmpbsa—A GROMACS Tool for High-Throughput MM-PBSA Calculations. J Chem Inf Model. 2014;54(7):1951-1962.
39. Humphrey W, Dalke A, Schulten K. VMD: Visual molecular dynamics. Journal of Molecular Graphics. 1996;14(1):33-38.
40. Kosar B, Albayrak C. Spectroscopic investigations and quantum chemical computational study of (E)-4-methoxy-2-[(p-tolylimino)methyl]phenol. Spectrochimica Acta Part A: Molecular and Biomolecular Spectroscopy. 2011;78(1):160-167.
41. Hay PJ, Wadt WR. Ab initio effective core potentials for molecular calculations. Potentials for K to Au including the outermost core orbitals. The Journal of Chemical Physics. 1985;82(1):299-310.
42. Investigation of coal structure. Office of Scientific and Technical Information (OSTI); 1993 1993/01/01.
43. Pearson RG. Absolute electronegativity and hardness:

application to inorganic chemistry. Inorganic Chemistry. 1988;27(4):734-740.
44. Geerlings P, De Proft F, Langenaeker W. Conceptual Density Functional Theory. Chem Rev. 2003;103(5):1793-1874.
45. Casida ME, Jamorski C, Casida KC, Salahub DR. Molecular excitation energies to high-lying bound states from time-dependent density-functional response theory: Characterization and correction of the time-dependent local density approximation ionization threshold. The Journal of Chemical Physics. 1998;108(11):4439-4449.
46. Brooks CL. Computer simulation of liquids. J Solution Chem. 1989;18(1):99-99.
47. Lobanov MY, Bogatyreva NS, Galzitskaya OV. Radius of gyration as an indicator of protein structure compactness. Mol Biol. 2008;42(4):623-628.
48. Luzar A, Chandler D. Hydrogen-bond kinetics in liquid water. Nature. 1996;379(6560):55-57.
49. Kollman PA, Massova I, Reyes C, Kuhn B, Huo S, Chong L, et al. Calculating Structures and Free Energies of Complex Molecules: Combining Molecular Mechanics and Continuum Models. Acc Chem Res. 2000;33(12):889-897.
50. Genheden S, Ryde U. The MM/PBSA and MM/GBSA methods to estimate ligand-binding affinities. Expert Opinion on Drug Discovery. 2015;10(5):449-461.